Instantaneous Frequency Estimation Method for the Vibration Signal of Rotating Machinery Based on STFTSC Algorithm

Binyun Wu

Department of Mechanical and Electrical Engineering, Xiamen University, Xiamen, 361102, China.

Shaojie Wang

Department of Mechanical and Electrical Engineering, Xiamen University, Xiamen, 361102, China.
Shenzhen Research Institute of Xiamen University, Shenzhen 518057, China. E-mail: wsj@xmu.edu.cn

Liang Hou, Xiangjian Bu, Chunhua Chen and Zheng Yang

Department of Mechanical and Electrical Engineering, Xiamen University, Xiamen, 361102, China.

(Received 3 November 2021; accepted 4 January 2022)

In this paper, an instantaneous frequency identification method known as STFTSC is developed by combining short–time Fourier transformation and the seam carving (SC) algorithm (widely used in image processing). In this method, the STFT is applied to analyze the time–frequency energy distribution of a vibration signal under variable-speed conditions. Subsequently, the energy gradient is calculated through the Sobel operator based on the time–frequency energy distribution. The energy gradient distribution contains multiple ridges, which are corresponding instantaneous frequencies of different orders. Finally, the targeted ridge extraction is transformed into an optimization problem, and the dynamic programming algorithm (DP) is used to search the targeted ridge with the minimum energy gradient to estimate the instantaneous frequency. The effectiveness of the proposed method is validated by a simulation experiment, moreover, a rotating machinery fault simulation test bench is employed to validate the method, which is then compared with polynomial chirplet transformation (PCT) and analyzed during the test process. The results show that the STFTSC instantaneous frequency estimation algorithm has a higher extraction accuracy and better application value in engineering problems than the PCT.

1. INTRODUCTION

With the rapid development in the production technology and equipment manufacturing industry, mechanical structures are becoming increasingly complex; key components, including bearings, gears, rotor systems, and other rotating components, are prone to failure. If these components fail, the normal operation of the entire equipment will be directly affected, resulting in huge economic losses and even casualties. Therefore, it is necessary to carry out an effective condition monitoring and fault diagnosis of the key components of mechanical equipment, find or predict symptoms that indicate deterioration, and take effective and timely measures to ensure the continuous, safe, and reliable operation of mechanical equipment. Conventional health monitoring and fault diagnosis methods for vibration signals are mainly based on the steady state, which is related to stationary signals. In practice, most rotating machinery operate under a non-stationary condition with variable speed and variable load. In this operation state, each stage is associated with varying speeds, and the vibration signal is essentially angular cyclostationary rather than time cyclostationary. Hence, the instantaneous fundamental frequency, on which the time–frequency analysis is based, varies. This makes frequency-based analysis tools effective only under constant-speed conditions. The instantaneous speed of rotating machinery not only reflects the characteristic parameters of its running state but also is an important parameter in variable-speed fault diagnosis methods such as time-varying filtering, generalized demodulation filtering, and order tracking. Methods that can help accurately obtain the instantaneous frequency corresponding to the rotation speed of the reference shaft are required for the health status assessment and early fault diagnosis of mechanical equipment under variable-speed conditions.[1–3]

For non-stationary signals under variable-speed conditions, time–frequency analysis[4,5] and order analysis[6–8] have been mainly used to extract eigenvalues. In the former approach, the transient characteristic information of the signal is obtained by applying a time–frequency analysis, whereas in the latter approach, the measurement information related to the rotation signal is extracted from a complicated signal, and the irrelevant interference signal is suppressed to find a relationship between the rotational frequency and the natural frequency of the rotor. Therefore, the order analysis method can consider the vibrations related to the speed and has evident advantages in the condition monitoring and fault diagnosis of complex equipment with variable speeds. However, In the conventional order analysis method, the instantaneous frequency should be accurately obtained using a tachometer in the process of order resampling and extraction of the order components. However, in practical engineering applications, because of the constraints of conditions and cost, no tachometer is provided, making it challenging to conduct the state monitoring and fault diagno-

sis. Because the vibration signals of complex equipment have certain regularity or periodicity, accurately extracting the instantaneous frequency from the signals through signal processing methods has emerged as a breakthrough approach, which can not only significantly reduce the monitoring cost and complexity of the system but also has important research value. Urbanek et al.[9] proposed a two-step method for estimating the instantaneous frequency with large fluctuations using the short-time Fourier transform (STFT) and ridge search algorithm. Aijun et al.[10] proposed an instantaneous frequency estimation method based on the improved peak search using STFT and a local peak search algorithm. However, the STFT calculates the spectrum of the vibration signal based on the assumption of local stationarity, that is, assumes that the extracted signal is stable in the analysis window, and then performs the Fourier transform on the extracted signal to generate the TFDs of the signal. Due to the restriction of the Heisenberg's uncertainty principle, the STFT cannot be able to achieve a fine resolution in both time and frequency domains, a good time resolution definitely implying a poor frequency resolution. Since the poor energy concentration of the time–frequency distributions, it is difficult for the STFT peak detection method to accurately extract the instantaneous frequency under the influence of noise and adjacent frequency interference. To this end, Yang et al.[11] proposed to estimate the instantaneous frequency based on the polynomial chirplet transform. However, the variation in the instantaneous frequency is irregular, because of which the order of the polynomial used for the fitting is high, resulting in the Runge phenomenon and thereby reducing the estimation accuracy. Rodopoulos et al.[12] proposed a harmonic decomposition parameter method for the instantaneous frequency, which is a parameter signal processing method based on eigenvalues. Its advantages include improved resolution and lower calculation cost. However, the accuracy of instantaneous frequency estimation under large background noise is insufficient. Ming et al.[13,14] proposed an instantaneous frequency estimation method based on the adaptive short-term chirp-Fourier transform by establishing an adaptive selection strategy for the frequency modulation parameters and then performing adaptive matching decomposition of the signal based on the time–frequency distribution characteristics. The method is robust to background noise signals; however, there is a trade-off between the speed estimation accuracy and the calculation efficiency. Therefore, it is necessary to establish a more accurate and reliable instantaneous frequency identification method for the variable-speed condition monitoring and fault diagnosis of complex equipment.

Seam carving (SC)[15,16] is an algorithm employed in the field of image processing to find the seam path (the best path) based on the energy gradient of the pixels in an image. This paper presents an STFTSC algorithm to accurately estimate the instantaneous frequency of rotating machinery under non-stationary conditions. In this method, the vibration signal under variable-speed conditions is taken as the research object, and it is transformed into the time–frequency energy distribution composed of time discrete points and frequency discrete points by short–time Fourier transform (STFT). Subsequently, the logarithm of the time–frequency energy spectral density is taken as the gray value of the pixel, and the SC algorithm is called to extract the instantaneous frequency. In this process, the energy gradient is calculated by Sobel operator, which contains multiple ridges, that is, the corresponding instantaneous frequencies of different orders. Finally, the targeted ridge with the minimum energy gradient is extracted by the DP algorithm to estimate the instantaneous frequency. The effectiveness of the proposed method in estimating the variable-speed instantaneous frequency is verified by a simulation test and a comparison of our method with the polynomial chirplet transform (PCT).

The rest of this paper is organized as follows. Section 2 presents the theory of the PCT proposed in reference[17] as well as the method and procedures used for instantaneous frequency estimation of the vibration signal. Section 3 introduces the STFT principle, the SC algorithm used to extract the seam path, and the STFTSC algorithm for an accurate estimation of the instantaneous frequency of the vibration signal of rotating machinery under variable-speed conditions. Section 4 presents a simulation test and an experimental study, performed to validate the effectiveness of the STFTSC algorithm, and a comparison of our method with the PCT algorithm to verify its accuracy. Finally, the conclusions drawn from the results are summarized in Section 5.

2. INSTANTANEOUS FREQUENCY ESTIMATION BY PCT

2.1. Principle of PCT

When the instantaneous frequency of a signal varies linearly with time, the conventional chirp wavelet transform can well describe the time–frequency distribution of the signal under appropriate frequency modulation parameters. However, when the instantaneous frequency trajectory is a nonlinear time-varying function, the conventional chirplet transform is inapplicable. For time domain signal $s(t)$, the PCT[17] is an improved algorithm proposed to solve this problem, and it is defined as follows:

$$\begin{aligned} &PCT_S(t_0,\omega,\alpha_1,\cdots,\alpha_n;\sigma) = \\ &\int_{-\infty}^{+\infty} z(t)\Phi^R_{\alpha_1\cdots\alpha_n}(t)\times \\ &\Phi^M_{\alpha_1\cdots\alpha_n}(t,t_0)\omega(\sigma)(t-t_0)\exp(-j\omega t)dt; \end{aligned} \tag{1}$$

and

$$\begin{cases} \Phi^R_{\alpha_1\cdots\alpha_n}(t) = \exp(-j\sum_{k=2}^{n+1}\frac{1}{k}\alpha_{k-1}t^k) \\ \Phi^M_{\alpha_1\cdots\alpha_n}(t,t_0) = \exp(j\sum_{k=2}^{n+1}\alpha_{k-1}t_0^{k-1}t) \end{cases}. \tag{2}$$

Where $z(t)$ is the analytical signal of $s(t)$, generated by the Hilbert transform $\boldsymbol{H}$, i.e., $z(t) = s(t) + jH[s(t)]$, $\Phi^R_{\alpha_1\cdots\alpha_n}(t)$ and $\Phi^M_{\alpha_1\cdots\alpha_n}(t,t_0)$ represent the nonlinear frequency rotation operator and the frequency shift operator, respectively, $\omega(\sigma)$represent the Gaussian window with time bandwidth σ, and $(\alpha_1,\cdots,\alpha_n)$ represented the polynomial kernel characteristic parameters, when $(\alpha_1,\cdots,\alpha_n) = (0,\cdots,0)$. Eq (1) can be simplified as:

$$\begin{aligned} &PCT_S(t_0,\omega,\alpha_1,\cdots,\alpha_n;\sigma) = \\ &\int_{-\infty}^{+\infty} z(t)\omega(\sigma)(t-t_0)\exp(-j\omega t)dt. \end{aligned} \tag{3}$$

This is equivalent to the normal STFT.

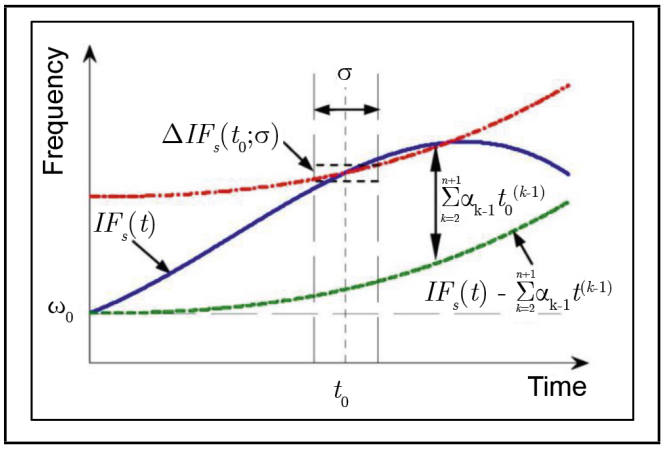

Figure 1. Illustration of the PCT (This image is taken from a previous study.[17])

The operating principle of the PCT is illustrated in Fig. 1, where $IF_s(t)$ was the IF trajectory of the analyzed signal. The specific steps are as follows:

1. First, the signal was rotated in the time–frequency plane by subtracting the IF of the analyzed signal, $IF_s(t)$.
2. The IF of the nonlinear chirp kernel, i.e., $\sum_{k=2}^{n+1}\alpha_{k-1}t^{(k-1)}$, was shifted by a frequency increment, $\sum_{k=2}^{n}\alpha_{k-1}t_0^{(k-1)}$.
3. Finally, the translated signal, as indicated by the red dotted line, was subjected to STFT with a window $\omega(\sigma)$.

2.2. Instantaneous Frequency Estimation by PCT

In the PCT, obtaining a set of appropriate polynomial kernel parameters was key to accurately identifying the instantaneous frequency of a rotating machinery vibration signal under a variable-speed condition from the time–frequency distribution of the signal. Based on the method proposed in reference[17], first, the initialization parameters $(\alpha_1,\cdots,\alpha_n)=(0,\cdots,0)$, threshold δ, and window width L were set. Subsequently, the time–frequency distribution of the signal is obtained using the PCT. Finally, the frequency corresponding to the location with the highest local energy in the time–frequency distribution was taken as the estimated instantaneous frequency, which is defined as:

$$\widetilde{IF}(t)=\arg\max_{\omega}[|PCT(t_0,\alpha,\beta,f,\omega;\sigma)|]. \tag{4}$$

where $\arg\max_{\omega}[f(x)]$ represented the operation of the set of variables x corresponding to the maximum value of the function $f(x)$. A new set of kernel parameters was obtained by polynomial curve fitting and then substituted into the next iteration. This process is repeated until the final iteration results meet the termination condition, and the termination condition can be set as:

$$Re=mean\left[\int\frac{\left|\widetilde{IF}_i(t)-IF(t)\right|}{IF(t)}dt\right]<\delta. \tag{5}$$

After the iteration, the optimal set of kernel parameters a_k $(k=0,1,\cdots,n)$ was finally obtained. The fundamental frequency polynomial of the vibration signal of the rotating machinery can be obtained using the following expression:

$$P_n(x)=\sum_{k=0}^{n}a_kx^k. \tag{6}$$

3. METHODOLOGY

3.1. Continuous Form of STFT

The spectrum of a random non-stationary signal varies with time; therefore, its local variation characteristics cannot be obtained using the conventional fast Fourier transform (FFT). In 1946, Gabor proposed the STFT, which was a time–frequency localized analysis method based on the FFT. The basic idea here was to use a fixed-size window function that slides over time to analyze non-stationary signals. We performed windowing and truncation processing, and assumed that the signal was stable within this window. The non-stationary signal can be decomposed into a series of approximately stationary short-term signals. Assuming that there was a window function $g(t)$ with a very short time width, the continuous STFT of the signal $x(t)$ can be defined as:[18]

$$S(t,f)=\int_{-\infty}^{+\infty}x(\tau)g^*(\tau-t)e^{-j2\pi f\tau}d\tau. \tag{7}$$

where $g^*(t)$ is a complex conjugate of $g(t)$. The function $S(t,f)$ contains both time-domain and frequency-domain information.

3.2. Discrete Form of STFT

In the process of analyzing the signal $x(t)$, since the collected signal was a discrete value, discretization was required when performing continuous STFT. The equation for the discrete STFT is as follows:

$$S(n\Delta t,f)=\sum_{k=-\infty}^{+\infty}x(k)g^*(k-n\Delta t)e^{-j2\pi kf}; \tag{8}$$

where $\Delta t=\frac{1}{f_z}$ was the sampling time interval, n was the time series, $x(k)$ was a discrete form of the signal $x(t)$, and $g(k)$ was the discrete form of the window function $g(t)$.

From Eq. (8), the discrete STFT result is a 2D complex matrix, containing the information of time and frequency. The STFT spectrum is defined as the square of the modulus of S, as shown in Eq. (9), which represents the time–frequency energy distribution, also known as the instantaneous frequency spectral density.

$$P(n\Delta t,f)=|S(n\Delta t,f)|^2. \tag{9}$$

3.3. Principle of Seam Carving Algorithm to Extract Seam Path

The SC algorithm was proposed by Shai Avidan of Mitsubishi Electric Research Laboratory and Ariel Shamir of interdisciplinary center and Mitsubishi Electric Research Laboratory in 2007. This method defines the energy function of an image based on the importance of its pixels, finds the seam path with the minimum energy, and then operates on this seam path to realize image scaling.[19–21]

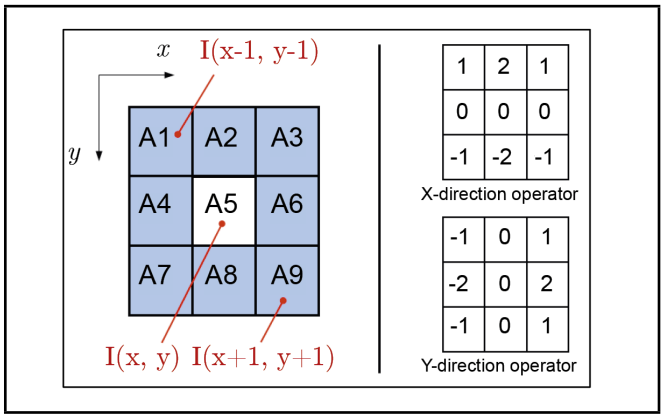

Figure 2. Gradient calculation template of Sobel operator.

To illustrate the process of extracting the seam path using the SC algorithm, an image with height n and width m is taken as an example; its pixel coordinate is (x, y), where $0 \leq x \leq (n-1)$, and $0 \leq y \leq (m-1)$. First, the energy distribution of the image is obtained, and the density function of the pixel (x, y) is defined as $I(x, y)$. Thus, the energy function (energy gradient distribution) of the pixel $e(I(x, y))$ can be expressed as:

$$e(I(x,y)) = |\frac{\partial}{\partial x}I(x,y)| + |\frac{\partial}{\partial y}I(x,y)| = |G_x(I(x,y))| + |\mathrm{G}_y(I(x,y))|. \quad (10)$$

The energy function is the modulus of the gradient of the grayscale image, which reflects the rate of grayscale change. Since a digital image in a computer is discrete, the derivative should be replaced by the difference when calculating the gradient modulus of its pixels. In practice, the gradient modulus operator is commonly used to calculate the gradient modulus. In this study, the Sobel operator, which is a better gradient modulus operator, is used to calculate the gradient modulus. The gradient of the central pixel is calculated using the surrounding 8 pixels by Sobel operator, and the higher weight is given to the points closing to the central pixel to highlight the central pixel. The gradient calculation template of the operator is shown in Fig. 2, where, the A5 was the central pixel. According to the template, the gradients in X and Y directions can be expressed as:

$$\frac{\partial I}{\partial x} = A1 + 2*A2 + A3 - A7 - 2*A8 - A9 = I(x-1,y-1) + 2I(x,y-1) + I(x+1,y-1) - I(x-1,y+1) - 2I(x,y+1) - I(x+1,y+1); \quad (11)$$

$$\frac{\partial I}{\partial y} = -A1 - 2*A4 - A7 + A3 + 2*A6 + A9 = -I(x-1,y-1) - 2I(x-1,y) - I(x-1,y+1) + I(x+1,y-1) + 2I(x+1,y) + I(x+1,y+1). \quad (12)$$

In the process of searching for the optimal seam, first, the fundamental frequency of rotating machinery was taken as the starting point of the minimum energy seam path. Second, a dynamic programming (DP) algorithm, namely a multi-stage optimization decision algorithm, was used to extract the optimal seam path, and the corresponding state transition equation is:

$$M(x,y) = e(I(x,y)) + \min\{M(x-1,y-1), M(x-1,y), M(x-1,y+1)\}; \quad (13)$$

where $M(x, y)$ was the sum matrix used to solve the dynamic programming, which represents the accumulative energy of the modified pixels at the coordinate points (x, y). Taking the vertical optimal seam as an example to extract the optimal seam path, we describe the following calculation process:

1. First, the energy function $e(I(x, y))$ of the image was calculated, and $M(1, y)$ was initialized to the value of $e(I(1, y))$. Thus, $M(1, y)$ was already the correct value. Subsequently, starting from the second line of $M(x, y)$, the value of this row was calculated from the value of the previous row based on Eq. (13).

2. After calculating the last row of M, if the pixel matrix corresponding to the minimum energy in this row was $P(m, y_1)$, it indicated that the path from the first row of the image to the coordinate point (m, y_1) was the path with the lowest energy in the image. Therefore, the pixel matrix with the optimal seam in the last row was $P(m, y_1)$.

3. Finally, the elements of the optimal seam in the other rows are traced backward. A marker matrix $Path(x, y)$ was used in the algorithm, and the calculation process was implemented using Eq. (14). Thus, based on the pixel matrix $P(m, y_1)$ and the marking matrix $Path(x, y)$, it can be inferred that the pixel matrix belonging to the optimal seam in the previous row was $P(m-1, y_1 + Path(m, y_1))$, and the path of the optimal seam can be traced in sequence.

Fig. 3 illustrates the implementation process of extracting the seam path based on the pixel matrix P and the mark matrix $Path$ i.e., to describe the process of extracting the optimal seam from the pixel (m_9, n_5) with the lowest energy in the last row to the first row using step (3).

3.4. Instantaneous Frequency Estimation by STFTSC Algorithm

In this study, we presented the STFTSC instantaneous frequency estimation algorithm by introducing the ideal of SC algorithm to search the best path combined with STFT and SC algorithm. Fig. 4 shows the flowchart of the method, with the vibration signal of a rotor in the rising speed stage taken as an example. The steps are as follows:

1. Time–frequency analysis of the vibration signal. First, the STFT was carried out on the vibration signal using Eq. (8) to obtain its time–frequency spectrum. Subsequently, the energy distribution of the time–frequency power spectrum, i.e., the instantaneous frequency spectral density, was calculated using Eq. (9).

2. Calculation of the energy function of the spectrum. In image processing, a gray image was obtained after gray

$$Path(x,y)=\begin{cases}-1 & \min\{M(x-1,y-1),M(x-1,y),M(x-1,y+1)\}=M(x-1,y-1)\\ 0 & \min\{M(x-1,y-1),M(x-1,y),M(x-1,y+1)\}=M(x-1,y)\\ 1 & \min\{M(x-1,y-1),M(x-1,y),M(x-1,y+1)\}=M(x-1,y+1)\end{cases}. \quad (14)$$

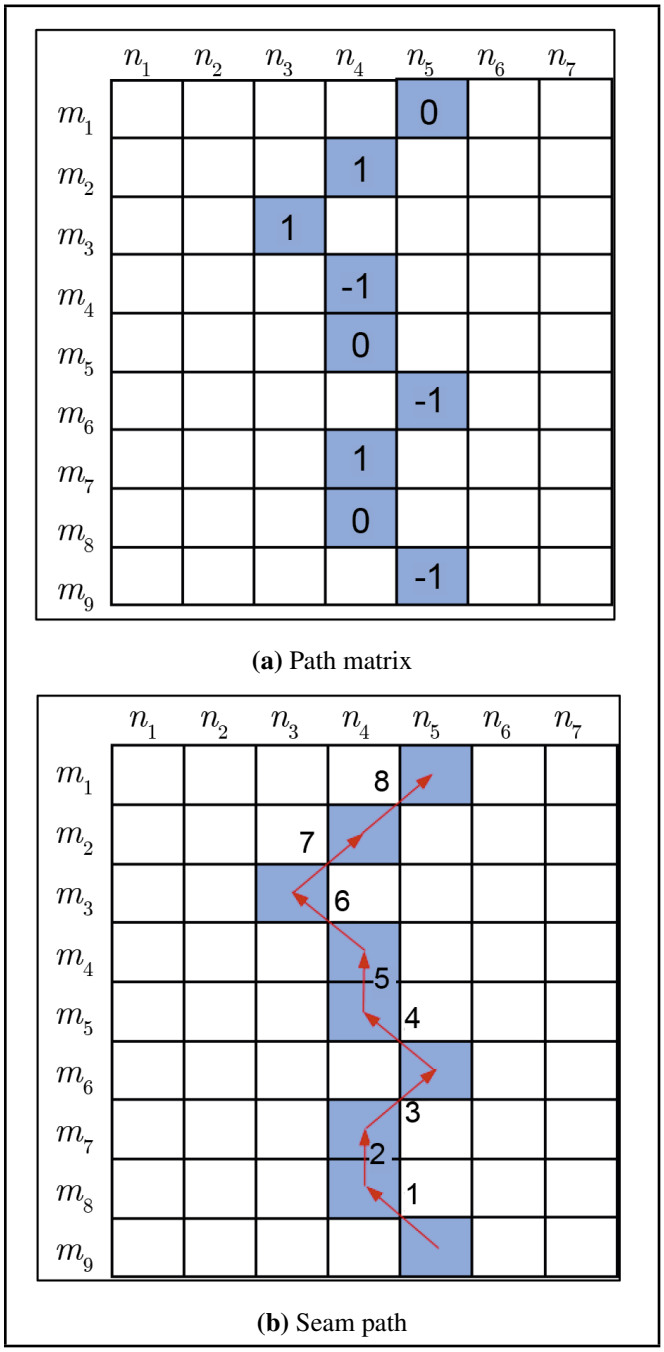

(a) Path matrix

(b) Seam path

Figure 3. Extraction process of seam path.

processing. Each pixel had only one gray value, which determines the brightness of the pixel, which was also called the energy of the pixel. In this study, the energy of the signal power spectrum is used to calculate the gradient, and the logarithm of the energy spectrum density obtained by the STFT transform was taken as the gray value of the pixel. The Sobel operator was then used to calculate the energy function $e(I(1,y))$ of the spectrum using Eq. (10). The energy gradient distribution contained multiple ridges, which were corresponding instantaneous frequencies of different orders.

3. Initial value selection. The lowest energy point at the edge of the energy sum matrix $M(x,y)$ was selected as the starting point of the targeted ridge; based on the theory of the algorithm, the frequency corresponding to this starting point is the instantaneous fundamental frequency of the rotating machinery.

4. Extraction of the targeted ridge. In general, the vibration signal contains noise and different frequency components. The noise and adjacent frequency interference were easy to cause the deviation between the local energy maximum and the real value of the time–frequency spectrum, which shows that the energy gradient of the time–frequency spectrum increases, resulting in discontinuous changes in the ridges of the same order in the time–frequency spectrum. Therefore, the ridge extraction was transformed into an optimization problem, and the targeted ridge with minimum energy gradient was extracted by using DP algorithm. The entire process can be represented by the state transition equation, namely Eq. (13), and the extraction process of the seam path (targeted ridge) shown in Fig. 3. For example, for a time–frequency spectrum energy matrix with time along the abscissa and frequency along the ordinate, the instantaneous frequency was extracted in the horizontal direction. Therefore, the matrix was transposed to extract the targeted ridge in the vertical direction. Thereafter, the matrix was transposed to ensure that the coordinates corresponding to the extracted instantaneous frequency are consistent with the original coordinates.

5. Extraction of the instantaneous frequency of the vibration signal. Based on the principle of the algorithm, the coordinate points corresponding to the targeted ridge extracted by the STFTSC algorithm were the coordinate points corresponding to the instantaneous frequency curve of the vibration signal. In other words, the curve drawn based on the corresponding coordinate points of the targeted ridge is the instantaneous frequency curve of the vibration signal to be extracted.

4. TEST VERIFICATION

4.1. Simulation Experiments

To verify the effectiveness of our method for instantaneous frequency extraction under the background of adjacent frequency interference and strong noise, a simulation test was carried out. In the actual test process of the variable-speed vibration signal of rotating machinery, it will inevitably be affected by the surrounding environment, resulting in the collected signal not only containing the fundamental frequency component and various noise components, but also mixed with different frequency components and various harmonics. Therefore, a multi–component signal model for the speed–up phase of rotating machinery was established through MATLAB program-

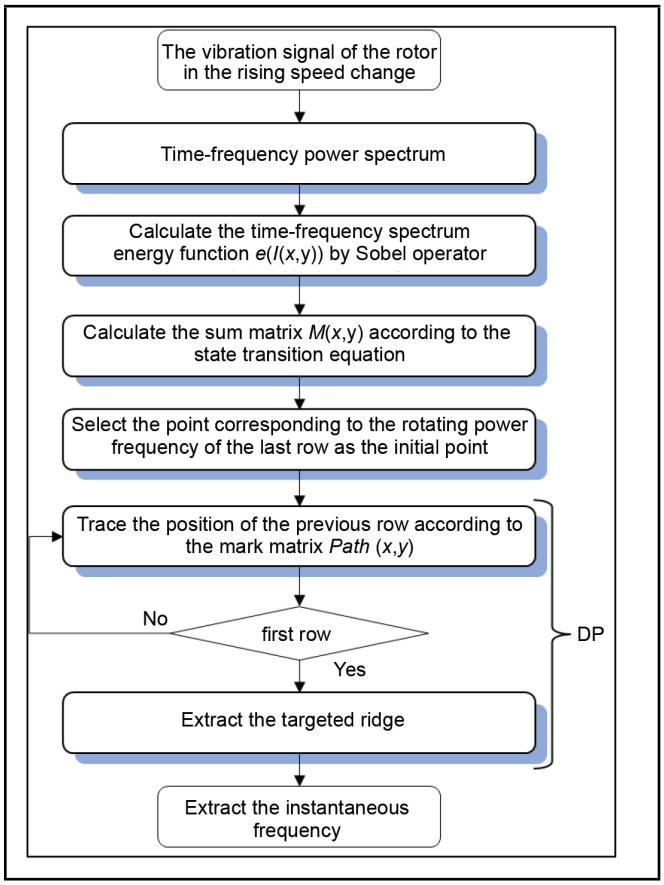

Figure 4. Flowchart of instantaneous frequency estimation by STFTSC algorithm.

ming, as follows:

$$x(t) = \sin\left(2\pi \int_{-\infty}^{t} \exp(\alpha\tau)d\tau\right) + 0.8\sin\left(2\pi \times 0.5 \int_{-\infty}^{t} \exp(\alpha\tau)d\tau\right) + 0.7\sin\left(2\pi \times 1.5 \int_{-\infty}^{t} \exp(\alpha\tau)d\tau\right) + 0.8\sin\left(2\pi \times 4 \int_{-\infty}^{t} \exp(\alpha\tau)d\tau\right) + \eta(t). \quad (15)$$

Where $\eta(t)$ was Gaussian white noise with a signal-to-noise ratio of 20%. The instantaneous frequency of the rotating machinery corresponding to the signal model can be expressed as:$\omega(t) = \exp(\alpha t)$, the sampling frequency of the signal was 200 Hz, and the sampling time was 25 s. Fig. 5 shows the time-domain curve of the original simulation signal. It can be seen from the figure that the relevant information such as instantaneous speed and time-frequency characteristics cannot be given in the figure due to the interference of measurement noise and non-stationary conditions.

Fig. 6 shows the STFT spectrum of the original signal, from which the signal contained 4 frequency components, among which the 0.5th, 1st and 1.5th order components are the adjacent order components. When the traditional STFT peak detection method is used to calculate the multi-component instantaneous frequency, it usually directly takes the extreme value of the time spectrum to get the corresponding discrete frequency points, and then uses polynomial fitting to get the instantaneous frequency estimation. However, this method was vulnerable to the interference of adjacent frequency and strong noise, resulting in a large deviation between the estimated instantaneous frequency and the real value, as shown in Fig. 7. The logarithm of the energy spectral density obtained by STFT was taken as the gray value of the pixel, and the first-order analysis frequency 42.52 Hz on the far right of the spectrum is selected as the starting point of the targeted ridge. Subsequently, the instantaneous change path (targeted ridge) of the first-order component was extracted by DP algorithm, as shown in Fig. 8(a). It can be seen from the figure that the identified optimal targeted ridge can well reflect the frequency change trajectory of the first-order component. The frequency coordinate points corresponding to the seam path were the instantaneous frequency estimation values of the variable-speed vibration signal to be extracted. It can be seen from Fig. 8(b) that almost all the instantaneous frequency estimation points fall on the actual instantaneous frequency curve. To compare the accuracy of these two methods to extract instantaneous frequency, Fig. 16 was used to calculate the relative error between the estimated instantaneous frequency and the actual instantaneous frequency. It was found that the error is 32.63% for traditional STFT spectral peak detection method, and the error of STFTSC is 0.69%. Therefore, STFTSC algorithm has high accuracy in extracting instantaneous frequency of rotating machinery vibration signal under variable-speed condition, which has high application value in engineering practice.

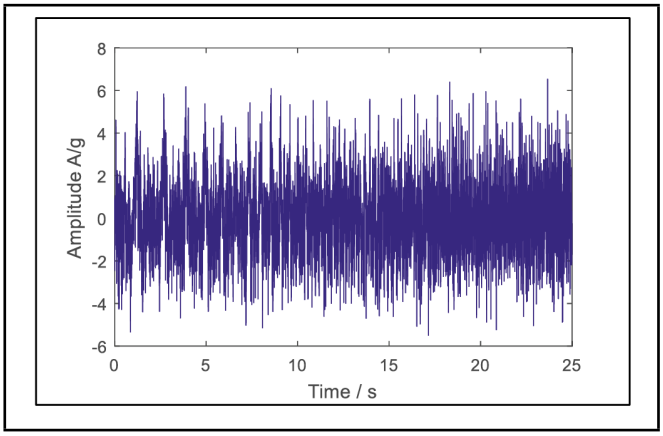

Figure 5. Time-domain curve of the simulation signal in the acceleration stage.

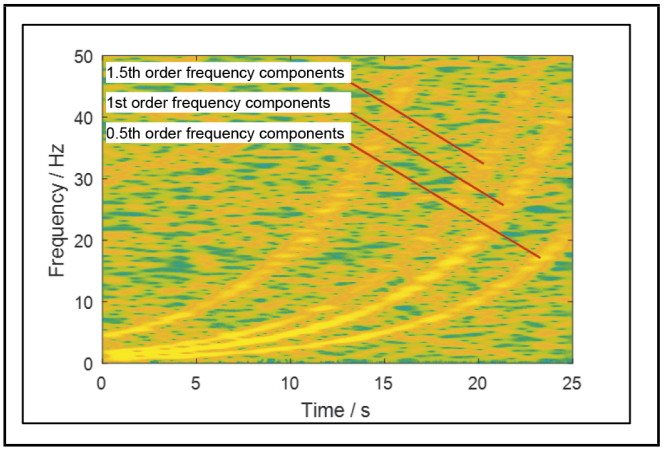

Figure 6. Time-frequency spectrum of STFT.

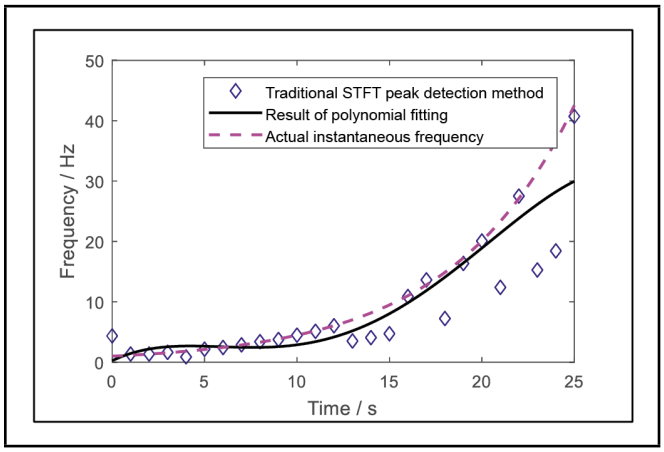

Figure 7. Extraction results of STFT peak detection method.

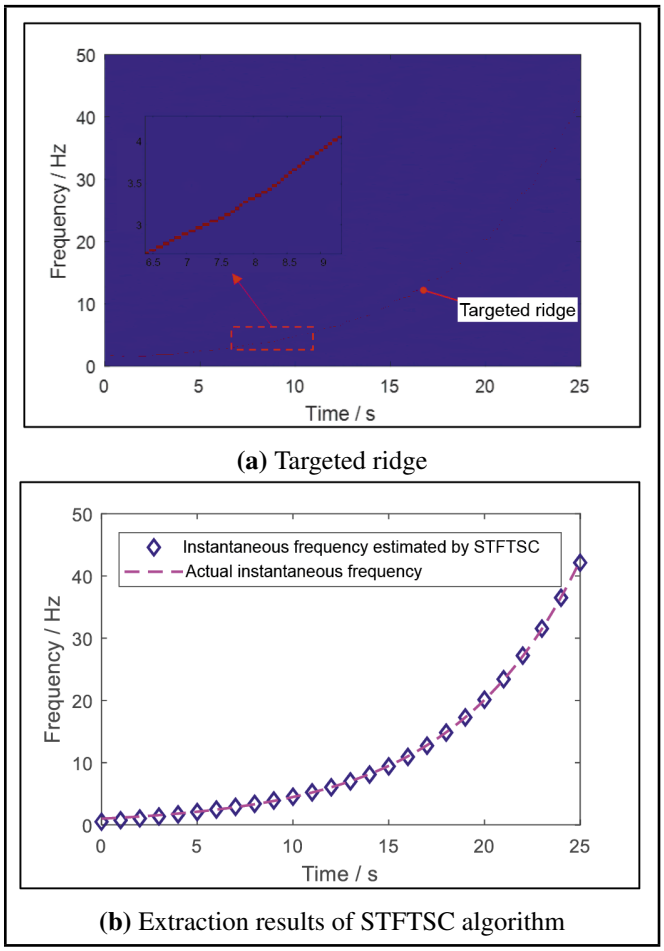

(a) Targeted ridge

(b) Extraction results of STFTSC algorithm

Figure 8. Extracting instantaneous frequency based on STFTSC algorithm.

$$\xi = \frac{\sqrt{\sum_{n=1}^{N}(f(n) - \hat{f}(n))^2}}{\sqrt{\sum_{n=1}^{N} f^2(n)}}. \tag{16}$$

Where $\hat{f}(n)$ was the estimated value of instantaneous frequency $f(n)$, and N was the number of instantaneous frequency points.

4.2. Application of Test Data

To further verify the effectiveness of the instantaneous frequency estimation method, the test method was verified.

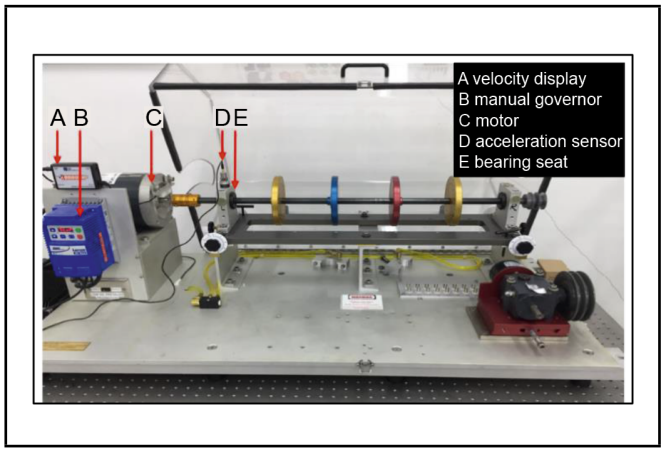

Figure 9. Mechanical fault comprehensive simulation test bench.

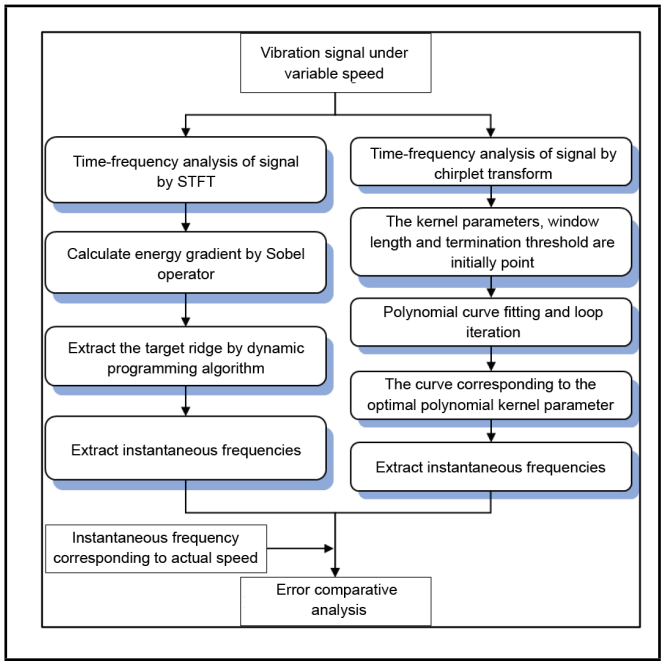

Figure 10. Flowchart of the test scheme

The test adopts the "Mechanical Failure Comprehensive Simulation Test Bench (MFS-MG)" produced by Spectraquest, USA.[22] The rotor test bed device is shown in Fig. 9, which mainly includes a velocity display, a manual governor, a drive motor, an acceleration sensor and a bearing seat. The rotor vibration signal under a variable-speed condition is obtained by controlling the speed change of the governor to simulate variable-speed conditions, and installing the acceleration sensor directly above the bearing seat. Fig. 10 shows the flowchart of the test scheme.

In general, the operating conditions of rotating machinery usually include acceleration stage, deceleration stage, and acceleration and deceleration stochastic stage. The vibration signals collected from these variable speed operating processes usually contain rich fault characteristics, which played an important role in the condition monitoring and fault diagnosis of rotating machinery. Limited by the internal control of rotor test bed, the working condition type of variable acceleration stage is selected for the test. Short time Fourier transform and polynomial chirplet transform as a typical representative of non-parametric and parametric time-frequency analysis methods,

PCT algorithm is widely used to extract effective eigenvalues in signal processing. Compared with STFT, when a set of appropriate polynomial kernel parameters are obtained, the time-frequency distribution obtained by PCT algorithm has higher energy concentration, which makes this method more effective in time-frequency analysis and feature extraction. Therefore, the PCT method with higher time–frequency energy concentration in the time–frequency distribution is selected to verify the superiority of the proposed method in this paper. The instantaneous frequency of the vibration signal collected from the rotor test bed in the variable acceleration stage was estimated. To verify the accuracy of this method in extracting the instantaneous frequency of the rotor vibration signal under a variable-speed condition, the method is compared with the PCT algorithm. In the acquisition process of the vibration signal under this condition, the rotor test bed is set to accelerate from 1200 rpm to 2400 rpm, and the corresponding theoretical value of the rotational fundamental frequency of the rotor system is increased from 20 Hz to 40 Hz. The sampling frequency of the signal was 256 Hz, and the sampling time is 20 s. It was inevitable to collect transient steady-state signals at the beginning and end of the acceleration stage, because of the short time of acceleration stage. To compare and verify the accuracy of the instantaneous frequency extracted using this method, the actual rotation speed of the rotating machinery was collected simultaneously.

Figs. 11(a), (b), and (c) show the time-domain curve of the vibration signal, the frequency spectrum in the 0–60 Hz range after FFT, and the instantaneous fundamental frequency variation curve corresponding to the actual speed of the rotor during the speed-up stage, respectively.

The spectrum (Fig. 11) shows that the frequencies of the two spectral peaks were 19.8 Hz and 39.7 Hz, corresponding to the rotor fundamental frequencies in the two stable stages, respectively, and the middle part was the fundamental frequency corresponding to the rotor speed-up stage.

To accurately estimate the instantaneous frequency of the rotor in the speed-up stage, first, a time–frequency analysis of the vibration signal is carried out through the STFT. When performing the STFT, the window width is selected as 256, and the length of the overlapped part of the window is 128. Fig. 12 shows the 3D spectrum of the STFT and time–frequency brightness spectrum of the vibration signal, from which the instantaneous change path of the fundamental frequency can be approximately distinguished. However, in the period of 8–14 s, the corresponding vibration signal presents a strong non-stationary behavior because the rotor is in the speed-up stage, resulting in a spectral ambiguity problem, which makes it difficult to extract the instantaneous frequency of the rotor under the variable-speed condition. The logarithm of the energy spectrum density obtained using the STFT is taken as the gray value of the pixel, and the rotational fundamental frequency of 39.7 Hz on the far right of the spectrum was selected as the starting point of the targeted ridge. The DP algorithm is used to extract the instantaneous change path (targeted ridge) of the fundamental frequency. As shown in Fig. 13(a), compared with Fig. 13(a) and Fig. 12(b), the two instantaneous frequency change paths are the same. Based on the corresponding coordinate points of the targeted ridge, the curve is the instantaneous change curve of the rotational fundamental frequency of the vibration signal to be extracted. The

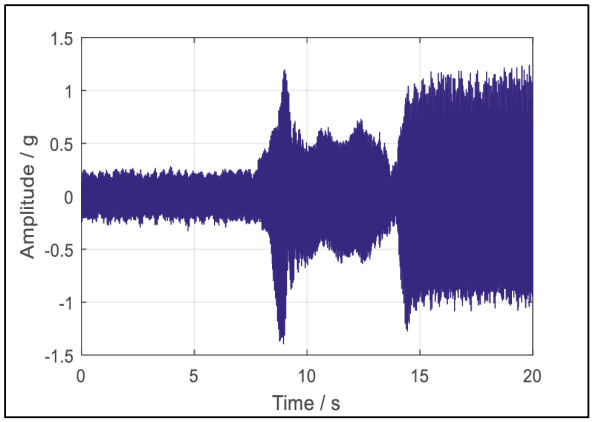

(a) Time-domain curve of the vibration signal

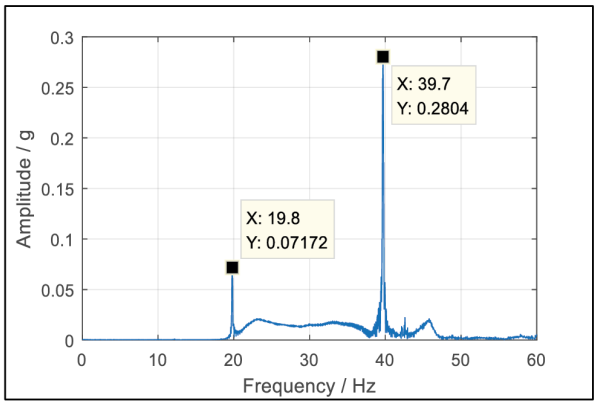

(b) Frequency-domain curve of the vibration signal

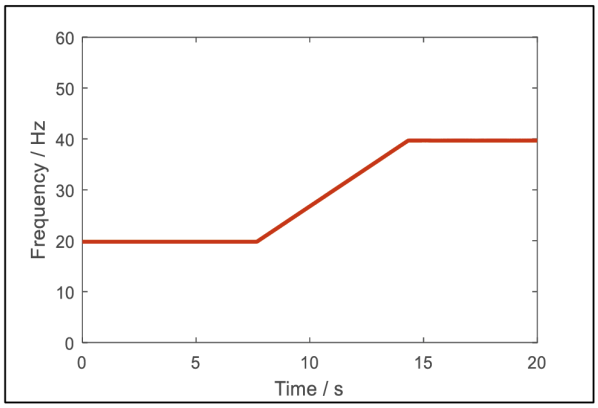

(c) Instantaneous variation curve of the actual rotational fundamental frequency

Figure 11. Time-domain curve, frequency spectrum, and actual instantaneous variation curve of the vibration signal.

extracted instantaneous fundamental frequency curve is resampled, and the curve is drawn, as shown in Fig. 13(b).

For a comparative analysis, the PCT algorithm is used to perform a time–frequency analysis of the vibration signal shown in Fig. 11(a). For the PCT, the Gaussian window is set to 512, the order of the polynomial kernel function was 15, and the termination condition is expressed in Eq. (16),[17] i.e., the average relative error between the next iteration result and the previous estimation value, and the termination threshold is set to 0.001. Fig. 14 shows the results of the time–frequency

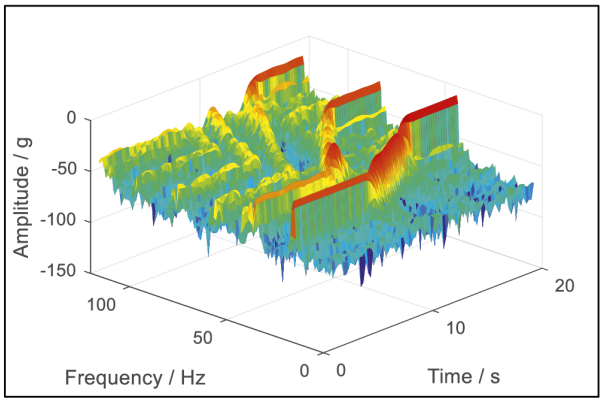

(a) Three-dimensional Time–frequency spectrum diagram

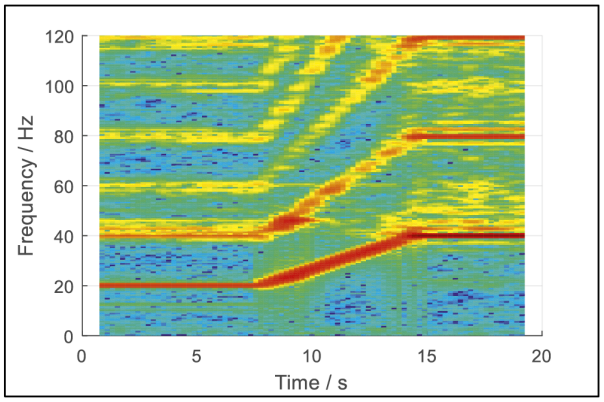

(b) Time-frequency brightness spectrum

Figure 12. Time-frequency distribution based on STFT.

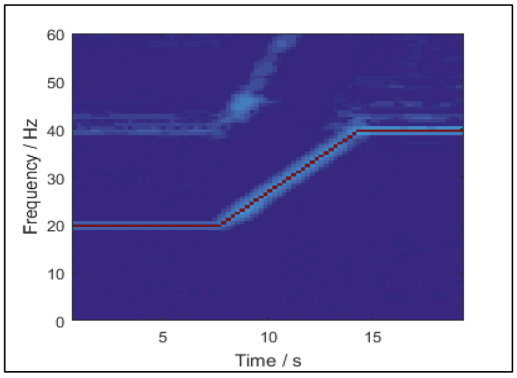

(a) Targeted ridge

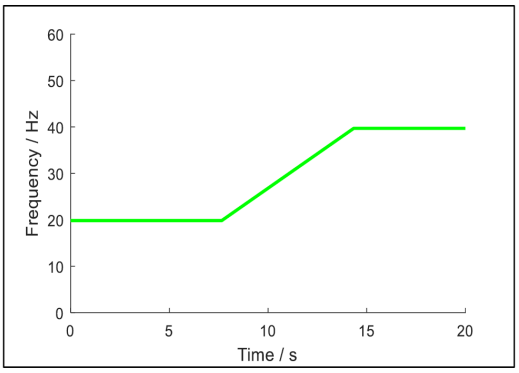

(b) Instantaneous transformation curve of fundamental frequency

Figure 13. Instantaneous change curve of the fault fundamental frequency extracted by STFTSC algorithm.

distribution of the signal. From the 3D time–frequency diagram and the 2D brightness spectrum, the time–frequency distribution transformed by the PCT algorithm has a better energy concentration, thus providing a better description of the non-stationary change process of the signal.

In the estimation of the parameters of the PCT, $(\alpha_0, \cdots, \alpha_{15}) = (0, \cdots, 0)$ is set as the initialization parameter, a set of new kernel function parameters is obtained by polynomial curve fitting, and the new kernel parameters are substituted into the next iteration. This process is repeated until the final iterative results meet the termination condition. Finally, after nine iterations, the fitted kernel function parameters of each order are obtained, and using the kernel function parameters of each order, the instantaneous fundamental frequency during the acceleration process of the rotor is approximated as expressed in Eq. (15). However, the variation in the instantaneous frequency is irregular, because of which the order of the polynomial used for the fitting is high, resulting in the Runge phenomenon and thereby reducing the estimation accuracy. The polynomial fitting curve of the instantaneous fundamental frequency is obtained, as shown in Fig. 15.

$$f(t) \approx 19.3315 + 4.5833t - 12.5372t^2 + 15.1840t^3 - 9.9832t^4 + 3.9742t^5 - 1.0209t^6 + 0.1756t^7 - 0.0206t^8 + 0.0016t^9 - 8.5069 \times 10^{-5}t^{10} + 2.5940 \times 10^{-6}t^{11} - 2.5575 \times 10^{-8}t^{12} - 1.0698 \times 10^{-9}t^{13} + 3.9775 \times 10^{-11}t^{14} - 4.1574 \times 10^{-13}t^{15}. \quad (17)$$

The STFTSC and PCT algorithm are compared in terms of their instantaneous frequency estimation results and estimation errors for the vibration signal of the rotating machinery under variable-speed conditions, as shown in Fig. 16. The fundamental frequency curve of the rotor rotation extracted by the two algorithms and the actual instantaneous fundamental frequency change curve largely coincide. The detailed enlarged figure shows that the instantaneous frequency extracted by the STFTSC algorithm is highly consistent with the actual conditions; the maximum error is less than 0.4%, and the root-mean-square error is 0.039 Hz. However, when the PCT algorithm is used, the extracted instantaneous frequency curve is obtained through a continuous iterative optimization, and the frequency spectrum obtained after the transformation exhibits edge ambiguity, which leads to a significant fluctuation in the extracted instantaneous frequency in the entire time interval. Even if the termination threshold is set to 0.001, the maximum error and root-mean-square error of the extraction are as high as 2.237% and 0.144 Hz, respectively, after nine iterations; Table 1 lists the result.

5. CONCLUSION

In the fault prediction and health management research of the key components of complex equipment, an accurately estimated instantaneous frequency corresponding to the reference shaft speed is the premise and foundation for ensuring the accuracy of condition monitoring and fault diagnosis of complex

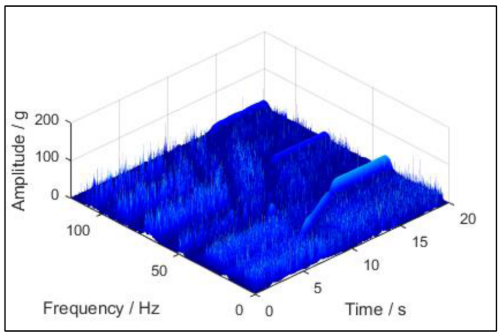

(a) Three-dimensional time-frequency diagram

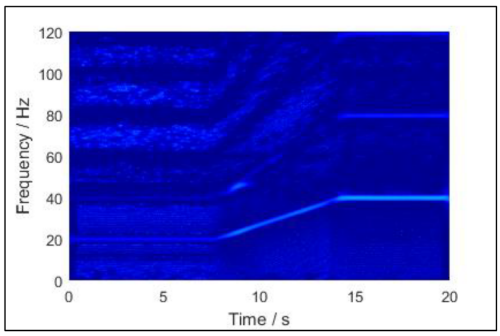

(b) Two-dimensional brightness spectrum

Figure 14. Time–frequency distribution based on the PCT algorithm.

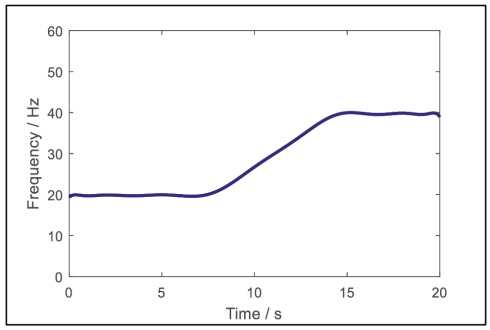

Figure 15. Instantaneous change curve of the fundamental frequency extracted by the PCT algorithm.

equipment under variable-speed conditions. Existing methods cannot accurately estimate the instantaneous frequency of rotating machinery under such conditions. Therefore, we established a more accurate and reliable instantaneous frequency identification method in this study. The following are the conclusions drawn from our research:

1. The principle of the time–frequency analysis based on the STFT was introduced in detail, and the implementation process of the SC algorithm for seam path extraction was discussed. By introducing the idea of seeking the optimal path in the SC algorithm, an STFTSC algorithm was developed by combining STFT with the SC algorithm. The algorithm was then applied to the instantaneous frequency estimation of the vibration signals of rotating machinery under variable-speed conditions.

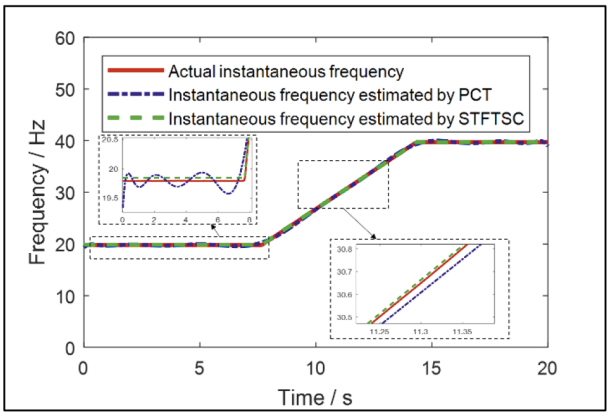

(a) Estimated result of the two algorithms studied

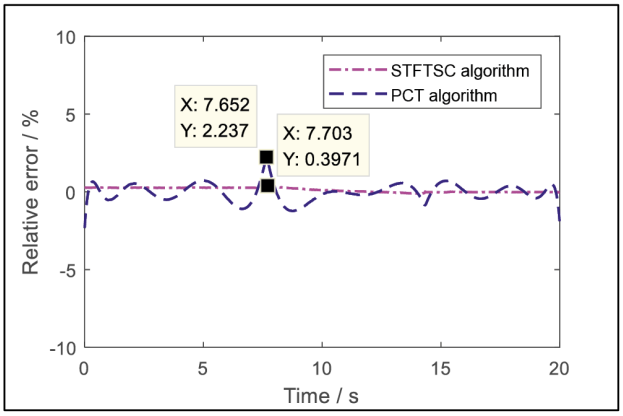

(b) Estimated error of the two algorithms studied

Figure 16. Comparison of the estimation results of the instantaneous fundamental frequency.

Table 1. Comparison of the estimation results of the instantaneous fundamental frequency

Method	STFTSC algorithm	PCT algorithm
Comparison of the maximum error between the estimated and actual results (%)	0.397	2.237
The root-mean-square error of the estimated and actual results (Hz)	0.039	0.144

2. To verify the accuracy of the proposed STFTSC algorithm in extracting the instantaneous frequency, a simulation experiment and an application experiment was designed to verify the method, and a comparison and analysis with the polynomial chirplet transform method were carried out. The comparison results showed that the proposed STFTSC algorithm has a higher accuracy and more application value in engineering practice.

The method discussed in this paper needs to be further verified on rotating machinery, which working conditions will be more complicated and the vibration signal noise will be stronger. Therefore, improving the algorithm's robustness and adaptability is the focus of future research work.

ACKNOWLEDGEMENTS

This work was supported by the National Key Research and Development Program (Grant No. 2020YFB1709901, 2020YFB1709904), the National Natural Science Foundation of China (Grant No. 51905460, 51975495), and Guangdong Basic and Applied Basic Research Foundation (Grant No. 2021A1515012286).

REFERENCES

[1] Ding, R., Shi, J., Jiang, X., Shen, C., and Zhu, Z., Multiple instantaneous frequency ridge based integration strategy for bearing fault diagnosis under variable speed operations, *Measurement Science and Technology*, **29**, 115002, (2018). https://dx.doi.org/10.1088/1361-6501/aada8c

[2] Takoutsing, P., Wamkeue, René, Ouhrouche, M., Slaoui-Hasnaoui, F., Tameghe, T., and Ekemb, G., Wind turbine condition monitoring: state-of-the-art review, new trends, and future challenges, *Energies*, **7**,2595–2630, (2014). https://dx.doi.org/10.3390/en7042595

[3] Peeters, C., Leclere, Q., Antoni, J., Lindahl, P., Donnal, J., and Leeb, S., Review and comparison of tacholess instantaneous speed estimation methods on experimental vibration data, *Mechanical Systems and Signal Processing*, **129**, 407–436, (2019). https://dx.doi.org/10.1016/j.ymssp.2019.02.031

[4] Lin, H., Gao, Z., Yi, C., and Lin, T., Simulation study on multi-rate time-frequency analysis of non-stationary signals, *Journal of Shanghai Jiaotong University (Science)*, **23**, 80–84, (2018). https://dx.doi.org/10.1007/s12204-018-1967-0

[5] Wang, L., Liu, S., Wei, M., and Hu, X., Time-frequency analysis of nonlinear and non-stationary weak signals of corona discharge, *Journal of Physics: Conference Series*, **418**, 12081–12081, (2013). https://dx.doi.org/10.1088/1742-6596/418/1/012081

[6] Randall, R., and Jérme A., Rolling element bearing diagnostics - a tutorial, *Mechanical Systems and Signal Processing*, **25** 485–520, (2011). https://dx.doi.org/10.1016/j.ymssp.2010.07.017

[7] Borghesani, P., Ricci, R., Chatterton, S., and Pennacchi, P., A new procedure for using envelope analysis for rolling element bearing diagnostics in variable operating conditions, *Mechanical systems and signal processing*, **38**, 23–35, (2013). https://dx.doi.org/10.1016/j.ymssp.2012.09.014

[8] Zhao, M., Lin, J., Xu, X., and Lei, Y., Tacholess envelope order analysis and its application to fault detection of rolling element bearings with varying speeds, *Sensors*, **13**, 10856–10875, (2013). https://dx.doi.org/10.3390/s130810856

[9] Urbanek, J., Barszcz, T., and Antoni, J., A two-step procedure for estimation of instantaneous rotational speed with large fluctuations, *Mechanical Systems and Signal Processing*, **38**, 96–102, (2013). https://dx.doi.org/10.1016/j.ymssp.2012.05.009

[10] Hu, A., and Zhu, Y., Instantaneous frequency estimation of a rotating machinery based on an improved peak search method, *Journal of Vibration and Shock*, **32**, 113–117, (2013). https://dx.doi.org/10.3969/j.issn.1000-3835.2013.07.023

[11] Yang, Y., Zhang, W., Peng, Z., and Meng, G., Multicomponent signal analysis based on polynomial chirplet transform, *IEEE Transactions on Industrial Electronics*, **60**, 3948–3956, (2013). https://dx.doi.org/10.1109/TIE.2012.2206331

[12] Rodopoulos, K., Yiakopoulos, C., and Antoniadis, I., parametric approach for the estimation of the instantaneous speed of rotating machinery, *Mechanical Systems and Signal Processing*, **44**, 31–46, (2014). https://dx.doi.org/10.1016/j.ymssp.2013.02.011

[13] Zhao, M., Lin, J., Wang, X., Lei, Y., and Cao, J., A tacholess order tracking technique for large speed variations, *Mechanical Systems and Signal Processing*, **40**, 76–90, (2013). https://dx.doi.org/10.1016/j.ymssp.2013.03.024

[14] Zhao, M., Lin, J., Liao, Y., and Cao, J., Instantaneous rotating speed estimation using adaptive short-time chirp-Fourier transform and its applications, *Journal of Mechanical Engineering*, **14**, 14–20, (2015). https://dx.doi.org/10.3901/JME.2015.14.008

[15] Dong, W., Zhou, N., Paul, J. C., & Zhang, X., Optimized image resizing using seam carving and scaling, *ACM Transactions on Graphics*, **28**, 125–132, (2009). https://dx.doi.org/10.1145/1618452.1618471

[16] Domingues, D., Alahi, A., and Vandergheynst, P., Stream carving: An adaptive seam carving algorithm, *IEEE International Conference on Image Processing*, 901–904, (2010). https://dx.doi.org/10.1109/icip.2010.5653984

[17] Peng, Z., Meng, G., Chu, F., Lang, Z., Zhang, W., and Yang, Y., Polynomial chirplet transform with application to instantaneous frequency estimation, *IEEE Transactions on Instrumentation and Measurement*, **60**, 3222–3229, (2011). https://dx.doi.org/10.1109/tim.2011.2124770

[18] Kwok, H., and Jones, D., Improved instantaneous frequency estimation using an adaptive short-time Fourier transform, *IEEE Trans. Signal Process*, **48**, 2964–2972, (2000). https://dx.doi.org/10.1109/78.869059

[19] Cui, J., Cai, Q., Lu, H., Jia, Z., and Tang, M., Distortion-aware image retargeting based on continuous seam carving model, *Signal processing*, **166**, 107242.1–107242.10, (2020). https://dx.doi.org/10.1016/j.sigpro.2019.107242

[20] Wei, J., Lin, Y., and Wu, Y. A patch analysis method to detect seam carved images, *Pattern Recognition Letters*, **36**, 100–106, (2014). https://dx.doi.org/10.1016/j.patrec.2013.09.026

[21] Zhao, X., Wu, J., and Zhou, Z., Instantaneous frequency estimation based on improved seam carving algorithm, *Journal of Nanjing University of Information science and Technology(Natural science Edition)*, **9**, 214–219, (2017). https://dx.doi.org/10.13878/j.cnki.jnuist.2017.02.015

[22] Spectra Quest Inc, Machinery fault simulator-magnum operation manual, (2012).